



HAL
open science

Fe-biochar as a safe and efficient catalyst to activate peracetic acid for the removal of the acid orange dye from water

Changjie Shi, Yong Wang, Kai Zhang, Eric Lichtfouse, Cong Li, Yunshu Zhang

► To cite this version:

Changjie Shi, Yong Wang, Kai Zhang, Eric Lichtfouse, Cong Li, et al.. Fe-biochar as a safe and efficient catalyst to activate peracetic acid for the removal of the acid orange dye from water. *Chemosphere*, 2022, 307, pp.135868. 10.1016/j.chemosphere.2022.135686 . hal-03753321

HAL Id: hal-03753321

<https://hal.science/hal-03753321>

Submitted on 18 Aug 2022

HAL is a multi-disciplinary open access archive for the deposit and dissemination of scientific research documents, whether they are published or not. The documents may come from teaching and research institutions in France or abroad, or from public or private research centers.

L'archive ouverte pluridisciplinaire **HAL**, est destinée au dépôt et à la diffusion de documents scientifiques de niveau recherche, publiés ou non, émanant des établissements d'enseignement et de recherche français ou étrangers, des laboratoires publics ou privés.

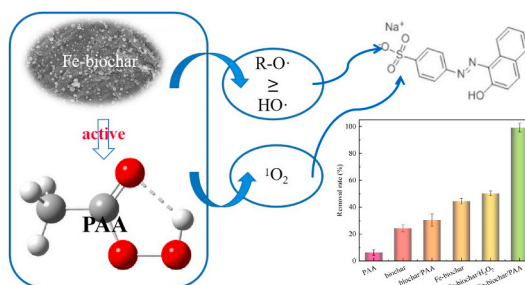
Fe-biochar as a safe and efficient catalyst to activate peracetic acid for the removal of the acid orange dye from water

Changjie Shi^a, Yong Wang^a, Kai Zhang^a, Eric Lichtfouse^b, Cong Li^{a,*}, Yunshu Zhang^a

^a School of Environment and Architecture, University of Shanghai for Science and Technology, Shanghai, 200433, China

^b Aix-Marseille Univ, CNRS, IRD, INRAE, CEREGE, Avenue Louis Philibert, Aix en Provence, 13100, France

- The mechanism of the Fe-biochar/PAA process was investigated by removing acid orange.
- $\text{CH}_3\text{C}(\text{O})\text{O}\cdot$ and $\text{CH}_3\text{C}(\text{O})\text{OO}\cdot$ act as the primary radicals.
- There may also be non-radical effects in the process of acid orange removal.
- Fe-biochar has a high recycling rate in the Fe-biochar/PAA process.



ABSTRACT

Pollution of wastewater and natural waters by organic contaminants is a major health issue, yet actual remediation methods are limited by incomplete removal of recalcitrant contaminants and by secondary pollution by chlorinated contaminants and catalytic metals. To attempt to solve these issues, we tested the removal of acid orange by peracetic acid (PAA), a safe oxidant, activated by Fe-biochar that iron anchored on biochar to prevent secondary pollution by iron. Fe-biochar was synthesized using a simple, one-step pyrolysis method. We investigated the effects of PAA concentration, pH, humic acids, chloride, bicarbonate on the reaction. Radical quenching and electron paramagnetic resonance were used to identify reacting species. Results showed that the granulous structure of Fe-biochar and the presence of Fe, Fe_3O_4 , Fe_2O_3 , and Fe_3C on Fe-biochar surface. The highest removal of acid orange of 99.9% was obtained with 1.144 mM PAA and 0.3 g/L Fe-biochar at pH 7. Acid orange removal increases with Fe-biochar dose, decreases with pH, is slightly inhibited by humic acids and bicarbonate, and is not modified by chloride. Our experimental results suggested that $\text{CH}_3\text{C}(\text{O})\text{OO}\cdot$ and $\text{CH}_3\text{C}(\text{O})\text{O}\cdot$ are the main radical species, but there may also be non-radical effects in Fe-biochar/PAA process. Fe-biochar displayed high re-usability, with 92.8% removal after five uses.

Keywords:

Transition metal catalyst (Fe-biochar)
Peracetic acid
Alkoxy radicals

* Corresponding author.

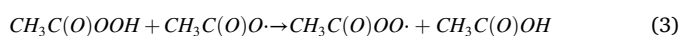
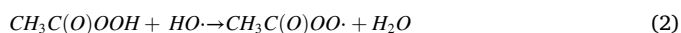
E-mail addresses: scj112233@yeah.net (C. Shi), yongw2021@163.com (Y. Wang), Kevin_ZhangK@126.com (K. Zhang), eric.lichtfouse@inrae.fr (E. Lichtfouse), congil@aliyun.com (C. Li), zhangys@usst.edu.cn (Y. Zhang).

1. Introduction

Peracetic acid (PAA) is a common oxidant with low toxicity generating few by-products, and has a high redox potential of 1.06–1.96 V. PAA has been extensively used in medical and health, agricultural construction, food production, beverage processing, and the textile industry (Monarca et al., 2002; Domínguez Henao et al., 2018; Jo et al., 2019; Silva et al., 2020; Tang et al., 2020). PAA spontaneously decomposes into reactive oxygen species at pH below 8.2, thus removing pollutants (Coyle et al., 2014). Therefore, PAA is considered as an alternative to chlorinated disinfectants. Nonetheless, PAA alone cannot remove most refractory organic pollutants. To solve this issue, the low peroxy bond energy, of 38 kcal mol⁻¹, of PAA can be activated by catalysis to generate highly reactive radicals such as HO· and R-O· (Rokhina et al., 2010; Rizzo et al., 2019; Ao et al., 2021). Such catalysis has been successfully applied to the removal of phenols (Rokhina et al., 2010; Ghanbari et al., 2021; Zhao et al., 2021), dyes (Zhou et al., 2015; Abd-Elhamid and Nayl, 2021; Yuan et al., 2021), and antibiotics (Wu et al., 2020; Chen et al., 2021; Liu et al., 2021) using various methods.

For instance, ultraviolet-catalyzed PAA removal of pharmaceuticals has revealed the presence of HO·, CH₃C(O)O· and CH₃C(O)-OO· (Cai et al., 2017). Ultrasound-catalyzed PAA and NaCl allows efficient microbial decontamination (Görgüç et al., 2021). Thermal activation of PAA also generates abundant free radicals (Wang et al., 2020a). Application of these methods at large scale is nonetheless limited by the cost of external energy. Alternatively, PAA can be activated by transition metals such as Fe²⁺ (Wang et al., 2020b, 2021b), Co²⁺ (Kim et al., 2020), Co₃O₄ (Wu et al., 2020), CoFe₂O₄ (Wang et al., 2021a), and Mn²⁺ (Rothbart et al., 2012) to generate free radicals such as HO· and R-O·, yet the recovery of those catalysts after reaction is difficult, thus inducing secondary pollution of natural waters. Safer energy-activated carbon materials can also be used to produce R-O· and HO· (Eqs. (1)–(3)), though the catalytic power is usually lower than metal catalysis which produce abundant R-O· with longer oxidation performance (Eqs. (4) and (5)). Therefore, research is actually focusing on anchoring metals on carbon materials to prevent metal leakage, to increase metal recyclability and to combine the catalytic effects of carbon and metals. In particular, cobalt salts has been anchored on carbon materials (Dong et al., 2022). Since cobalt is toxic and costly, here we hypothesized that anchoring iron salts on a carbon material would produce an efficient and safer catalysis. A one-step co-precipitation method has been studied to synthesize magnetic sludge -derived biochar and use it to activate persulfate to remove acid orange7 (Wang et al., 2017). However, relevant research on PAA activation has not yet appeared.

We report here the synthesis of Fe-biochar by simple pyrolysis, and the activation of PAA by Fe-biochar to remove the acid orange dye from water. We characterized the structure of Fe-biochar and we tested the effects of PAA concentration, pH, humic acids, chloride, bicarbonate on the reaction. The reaction mechanism was studied by radical quenching and electron paramagnetic resonance to identify radicals. The stability of the synthetic materials was evaluated. The study will provide reference for the development of activated PAA technology that can be practically applied to advanced treatment of drinking water or sewage.



2. Materials and methods

2.1. Chemicals

The raw material of biochar is wheat straw provided by a farmland in Jining, Shandong. Acid orange and 15–20% PAA are from Aladdin Reagent Co, Shanghai. Supplementary Text S1 report the sources of other chemical reagents. All chemicals are of analytical grade. All solutions were prepared by deionized water.

2.2. Experimental procedures

Wheat straw was soaked 48 h in 0.2 mol/L NaOH for removing ash, wax and impurities on the surface of it. Then washed with deionized water until neutral, dried and grinded until it could pass through a 100-mesh sieve, then dried and stored for later use. Straw powder (6 g every time) was dipped 6 h into the 30% Fe(NO₃)₃·9H₂O, filtered and dried at 60 °C until constant weight. Then, the 2 g straw powder was pyrolyzed 2 h in a tube furnace (700 °C) with nitrogen flow to produce Fe-biochar which was water-washed and 70% ethanol-washed (remove small molecular organics), dried, sealed and stored for later use.

All reactions were performed in 250 ml glass conical flasks with 400 rpm stirring at 23 ± 2 °C. PAA, H₂O₂ and Fe-biochar or biochar were added to 200 ml of 50 mg/L acid orange solution, then 2 mL samples were taken out with a syringe at different times and quickly quenched in excess Na₂S₂O₃ solution. The pH of the initial solution was adjusted by adding 0.2 mol L⁻¹ NaOH or 0.1 mol L⁻¹ H₂SO₄ to the solution. Free radical scavengers were ascorbic acid, *tert*-butyl alcohol (TBA), methanol and 2,4-hexadiene (2,4-HD). In the experiments of different influencing factors, the corresponding chemical agents were added before the reaction. As for the catalyst cycling tests, Fe-biochar was collected by suction filtration (0.45 μm) and washed with deionized water for three times, then dried under vacuum condition at 40 °C. PAA concentration was determined periodically. All experiments were at least repeated or performed multiple times.

2.3. Analytical methods

PAA concentration was measured by iodimetry (Chen et al., 2019). The residual concentration of PAA during the experiment was determined by N, N-diethyl-p-phenylenediamine colorimetric method (Cavallini et al., 2013). The content of H₂O₂ was determined by the titanium potassium oxalate method (Yang et al., 2018). pH was monitored by a pH meter PHSJ3 from Leici, Shanghai. The concentration of acid orange was analyzed by spectrophotometry. The free radicals were measured by electron paramagnetic resonance (EPR) analysis using 5,5-dimethyl-1-pyrroliidone-N-oxyl (DMPO) and 2,2,6,6-Tetramethyl-1-piperidinyloxy (TEMP) as the trapping agent. The surface features and internal crystal structure of the samples were analyzed by the scanning electron microscope (SEM, ZEISS Sigma 500, Germany) and transmission electron microscope and high-resolution transmission electron microscope (TEM and HRTEM, FEI talos f200s, America). X-ray diffraction (XRD) patterns of samples were analyzed by X-ray diffractometer (Bruke D8 Advance, Germany) with Cu Kα radiation. N₂ adsorption-desorption curve was analyzed at 77 K (ASAP 2020, America) and the specific surface areas and pore diameter were measured by the standard Brunauer–Emmett–Teller (BET) method. The dissolved iron concentration was measured by ICP-OES (Optima8000, PerkinElmer, US).

3. Results and discussion

3.1. Characterization of Fe-biochar and biochar

We compared the structure of biochar and Fe-biochar by scanning electron microscopy (SEM, Fig. 1). At low magnification of 20 μm, biochar displays hollow cavities that should be suitable for loading Fe

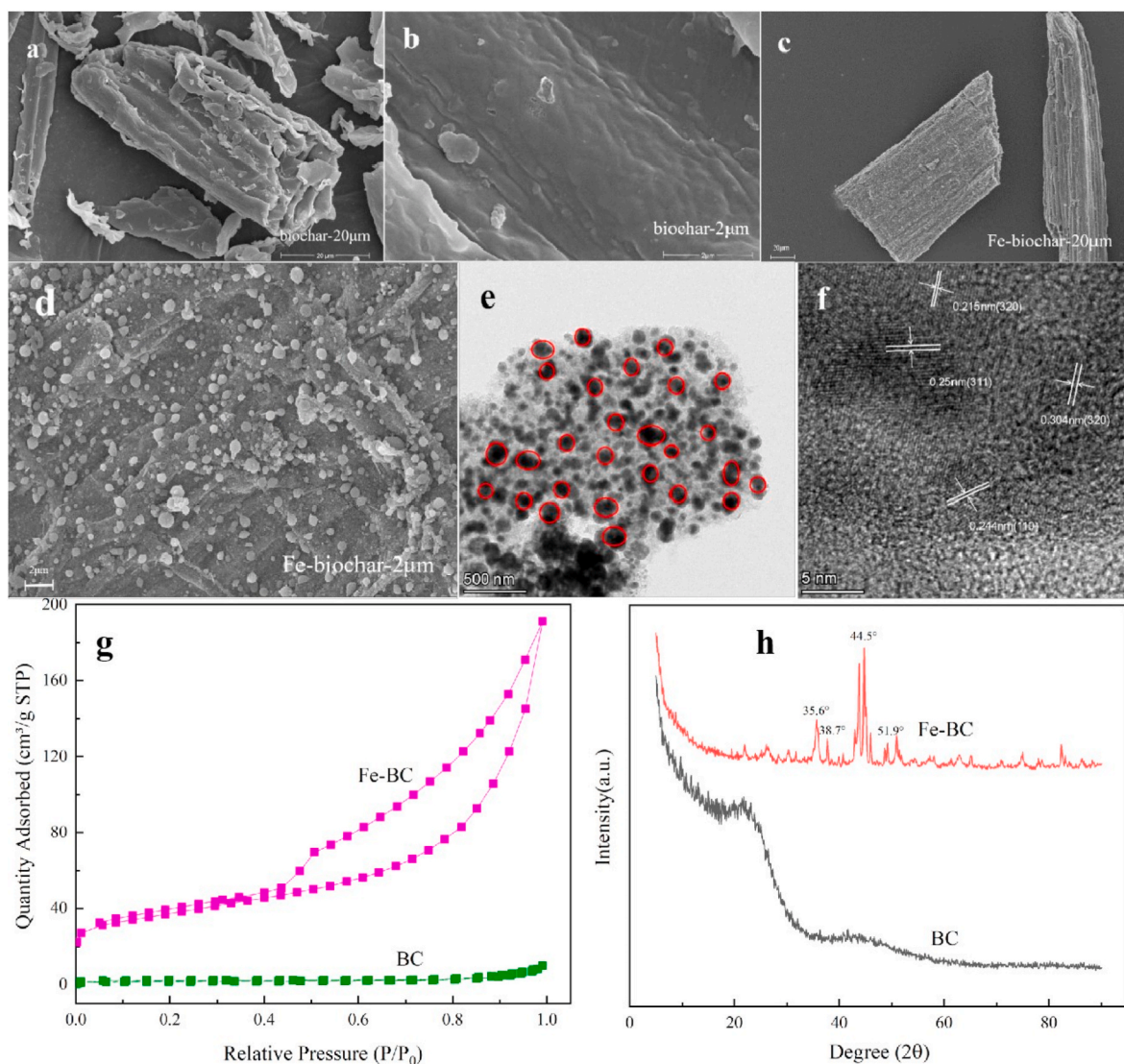


Fig. 1. The SEM images of (a) biochar (2 μm), (b) biochar (20 μm), (c) Fe-biochar (2 μm), (d) Fe-biochar (20 μm), (e) TEM image and (f) HRTEM image of Fe-biochar, (g) N₂ adsorption-desorption isotherm curves of biochar and Fe-biochar, (h) XRD patterns of biochar and Fe-biochar.

catalytic compounds (Fig. 1a). Both biochar and Fe-biochar has a similar layered structure of this scale (Fig. 1a, c). At high magnification of 2 μm, biochar has a smooth surface, whereas Fe-biochar displays numerous small granules, which likely result from the FeNO₃·9H₂O treatment before biochar pyrolysis. Analysis of Fe-biochar by transmission electron microscopy (TEM) reveals dispersed granules at low magnification of 500 nm (Fig. 1e). Interplanar spacings between adjacent lattice fringes reveals the presence of Fe₂O₃ (320) at 0.215 nm, Fe (110) at, 0.244 nm, Fe₃O₄ (311) at 0.250 nm and Fe₃C (221) at 0.304 nm (Fig. 1f).

Analysis by X-Ray diffraction confirms the presence of Fe at 44.5°, Fe₂O₃ at 38.7°, Fe₃O₄ at 35.6°, and Fe₃C at 51.9° in Fe-biochar versus raw biochar (Fig. 1g). According to peak intensity, the relative abundance of Fe compounds is in decreasing order: Fe, Fe₃O₄, Fe₂O₃, and Fe₃C. N₂ adsorption/desorption isotherms at high pressure, of P/P₀ higher than 0.5, reveal hysteresis loop for Fe-biochar (Fig. 1f). This isotherm type indicates a mesoporous structure (Ahmad et al., 2019). The specific surface area of Fe-biochar before the activation, of 128.36 cm²/g, is lower than that of biochar, of 146.15 cm²/g (Table S1). This might be due to the presence of Fe compounds in Fe-biochar pores, and to the stacking of biochar flakes around Fe compounds. The addition of iron also enlarged the pore volume from 0.06 to 0.29 cm³/g, and pore size from 2.5 to 8.0 nm of biochar (Table S1). Overall, our findings

reveal the granulous structure of Fe-biochar and the presence of Fe, Fe₃O₄, Fe₂O₃, and Fe₃C on Fe-biochar surface. At low relative pressure, it was similar to the type II curve, while at higher pressure (P/P₀ > 0.5), capillary condensation occurred in Fe-biochar with a hysteresis loop. This isotherm type corresponded to the mesoporous structure (Ahmad et al., 2019). In contrast, the curve change of biochar was weak, and the trend was closer to type II. It belongs to the microporous structure in terms of pore volume and pore size.

3.2. Removal of acid orange

We tested the removal of acid orange with PAA, biochar, biochar and PAA, Fe-biochar, Fe-biochar and H₂O₂, and Fe-biochar and PAA in distilled water (Fig. 2). Results show that PAA alone induces the lowest removal of 6.3% after 25 min of reaction. This suggests that PAA alone has little oxidizing power, and agrees with the fact that PAA reacts poorly with electron-withdrawing groups (Kim and Huang, 2021). Biochar alone induces a slightly higher removal of 24.2%, which is likely explained mainly by adsorption of acid orange on biochar surface. A study also verified that biochar has a limited capacity and takes a long time to adsorb acid orange (Huang et al., 2020). Biochar and PAA induce a slightly higher removal of 30.5%, which suggests an additive

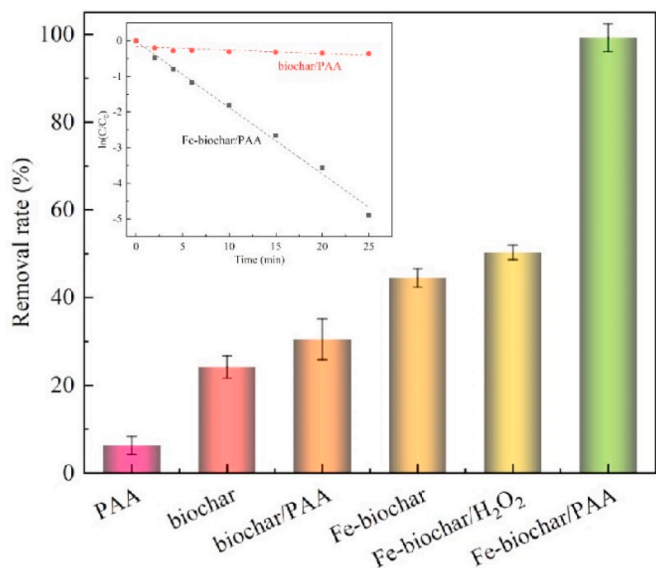
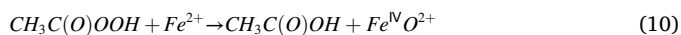
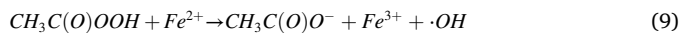
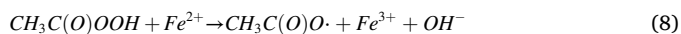


Fig. 2. Removal of acid orange under different processes. $[\text{acid orange}]_0 = 0.143 \text{ mM}$, $[\text{PAA}]_0 = [\text{H}_2\text{O}_2]_0 = 1.144 \text{ mM}$, $[\text{catalysts}]_0 = 0.3 \text{ g/L}$, $\text{pH} = 7.0$.

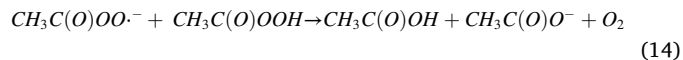
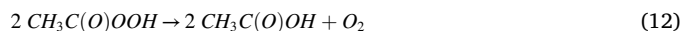
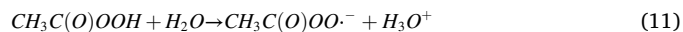
contribution of biochar adsorption and PAA oxidation. Remarkably, all materials containing iron display higher removals, of 45.5% for Fe-biochar, 49.7% for Fe-biochar and H_2O_2 , and 93.3% for Fe-biochar and PAA. This indicates that a major part of acid orange removal is due to catalytic transformation induced by Fe species. Possible products include acid orange radicals and various removal products, which may be adsorbed on Fe-biochar or mineralized to CO_2 .



The slight removal improvement from 45.5% for Fe-biochar to 49.7% for Fe-biochar and H_2O_2 results probably from direct H_2O_2 oxidation and H_2O_2 , activation by Fe (Eq. (6) and (7)). To further study the effect of H_2O_2 , different concentrations of H_2O_2 were added to the Fe-biochar/PAA/AOII process, as shown in Fig. S1. H_2O_2 with higher concentration will inhibit the degradation effect of Fe-biochar/PAA. And we suspect that H_2O_2 will quench the formed free radicals, which was also confirmed by Wang et al. (2020c). Therefore, the degradation of AOII was due to the activation of PAA by Fe-biochar. By contrast, the high removal improvement from 45.5% for Fe-biochar to 93.3% for Fe-biochar and PAA likely results from the strong activation of PAA by Fe (Eqs. (8)–(10)) followed by removal of acid orange, which might partly favor adsorption of products on biochar. This finding agrees with the high reactivity of a mixture of Fe(II) and PAA (Kim et al., 2019). The highest removal with to 93.3% for Fe-biochar and PAA is also supported by our results on the higher decomposition of PAA with Fe-biochar versus biochar and PAA alone (Fig. S2). Our further study of the optimal concentrations of Fe-biochar and PAA showed that a Fe-biochar dose of 0.3 g/L and a PAA concentration of 1.144 mM induced the highest removal of 99.8% (Text S2, Figs. S3 and 4). Overall, anchoring Fe onto biochar induced a substantial increase of acid orange removal. This is explained by activation by Fe species anchored on the biochar, followed by removal of acid orange then possible adsorption of acid orange products on biochar.

3.3. Effect of pH

We studied the effect of pH on the removal of acid orange by Fe-biochar and PAA. Results show that acid orange removal in decreasing with pH, from 99.5% at pH 3–83.4% at pH 11 after 20 min of reaction (Fig. 3). The corresponding removal rates decrease from 0.2804 min^{-1} at pH 3 to 0.0519 min^{-1} at pH 11 (Fig. S5). After 20 min, curiously, the removal decreases at pH 9 and 11, which can first be partly ascribed to the reduction of active species induced by the decomposition and hydrolysis of PAA (Eq. (11)–(13)). Second, another explanation is the formation of peracetate radicals in alkaline conditions, which can in turn consume PAA (Eq. (14)), similarly to reports on the removal of naproxen with UV and PAA (Zhang et al., 2017; Chen et al., 2019). Third, Fe species anchored on biochar are likely to form complexes in alkaline conditions, similarly to the formation of cobalt hydroxide complexes that inhibit reactions (Zhang et al., 2021b). Fourth, the Fenton reaction involving Fe^{2+} activation of PAA works better under acidic conditions, as shown for the removal of methylene blue (Yuan et al., 2021). Fifth, alkaline conditions should decrease the adsorption of acid orange onto Fe-biochar following the formation of more anions both on acid orange and on Fe-biochar, and in turn increase electrostatic repulsion. This would agree with the fact that the most efficient method to extract humic substances, e.g. from soils, involves alkaline extraction (Mohi-nuzzaman et al., 2020). Overall, we found that acid orange removal decreases with pH and is possibly explained by removal of PAA, inactivation of Fe catalytic sites of Fe-biochar by formation of Fe hydroxydes and less adsorption of acid orange onto Fe-biochar due to formation of anionic groups.



3.4. Effect of humic acids, HCO_3^- and Cl^- on acid orange removal

In Fig. 4, it was obvious that humic acids and HCO_3^- has an inhibitory

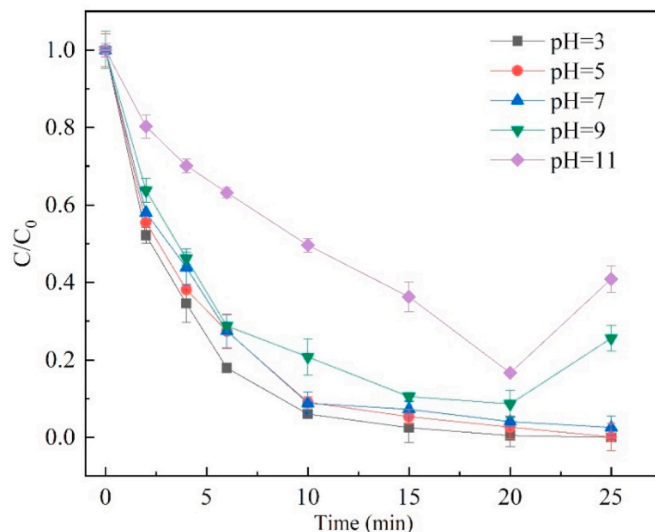


Fig. 3. (a) Effect of initial pH on the removal of acid orange in the Fe-biochar/PAA process. $[\text{acid orange}]_0 = 0.143 \text{ mM}$, $[\text{PAA}]_0 = 1.144 \text{ mM}$, $\text{Fe-biochar}_0 = 0.3 \text{ g/L}$. (For interpretation of the references to color in this figure legend, the reader is referred to the Web version of this article.)

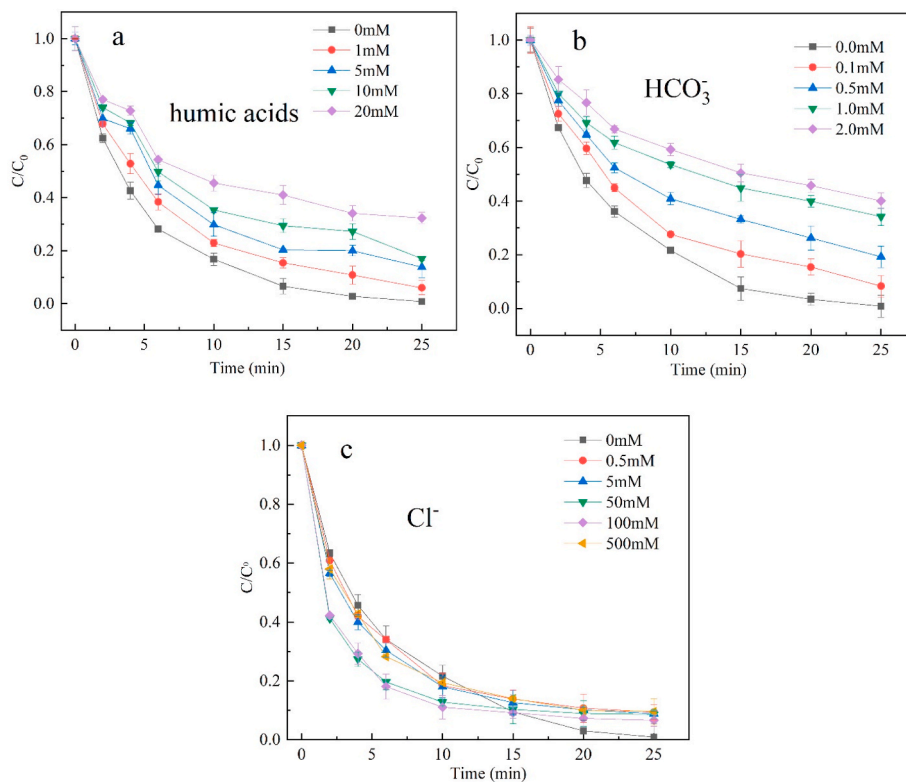
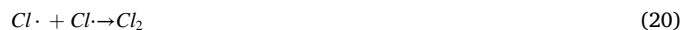
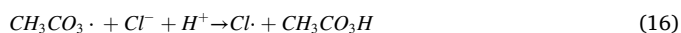


Fig. 4. Effect of (a) humic acids, (b) HCO_3^- and (c) Cl^- on the removal of acid orange in the Fe-biochar/PAA process. $[\text{acid orange}]_0 = 0.143 \text{ mM}$, $[\text{PAA}]_0 = 1.144 \text{ mM}$, $\text{Fe-biochar}_0 = 0.3 \text{ g/L}$, $\text{pH } 7.0$. (For interpretation of the references to color in this figure legend, the reader is referred to the Web version of this article.)

effect on the removal of acid orange under the Fe-biochar/PAA process. The decomposition of PAA was also investigated in the presence of humic acids in Fig. S6, which showed the amount of decomposition of PAA was significantly reduced, indicating that the addition of humic acids affected the effect of PAA. It was reported that humic acids can compete with acid orange and O_2 for electrons (Chen et al., 2021) and inhibit the activation of PAA, the formation of free radicals and the scavenging of acid orange. In addition, humic acids can react with $\text{R-O}\cdot$ with the rapid reaction rate constant of $1 \times 10^4 \text{ L mg}^{-1} \text{ s}^{-1}$ (Chen et al., 2019). The inhibitory effect of HCO_3^- was partly attributed to the formation of unreactive cobalt-bicarbonate complexes. The similar results were also found on the removal of SMX in the Co/PAA process (Wang et al., 2020c). Besides, HCO_3^- can react with radical species in Eq. (15), inhibiting the removal of acid orange. The result is consistent with the UV/PAA process (das Neves et al., 2021). As shown in Fig. S6, the decomposition of PAA in the Fe-biochar/PAA process with HCO_3^- was inhibited, which indicated that the formation of unreactive iron-bicarbonate complexes. In Fig. 4c, the effect of Cl^- on the removal of acid orange could be ignore. Cl^- can react with radical species as Eq. (16)–(20). As shown in Fig. S6, the addition of Cl^- had a negligible effect on the decomposition of PAA in the Fe-biochar/PAA process before 10 min, but in the end, it will affect the total amount of decomposition. Low concentration of Cl^- is not sufficient to affect the Fe-biochar/PAA process and the reaction of high concentration of Cl^- and radical species to form $\text{Cl}\cdot$ will also accelerate the removal of acid orange (Görgüç et al., 2021). The intermediate concentration of Cl^- inhibited the removal of acid orange to a certain extent due to the inhibition of $\text{R-O}\cdot$ and $\text{HO}\cdot$.



3.5. Reactive species accounting for acid orange removal in the Fe-biochar/PAA process

In Fig. 5a, ascorbic acid significantly decreases the removal rate of acid orange (38.1%) compared with without ascorbic acid (99.3%) in the same conditions. Ascorbic acid is a typical free radical scavenger, which was used to initially investigate whether the removal of acid orange in Fe-biochar/PAA process was caused by free radicals. Since the catalyst played a dominant role in the reaction, further research found that the addition of ascorbic acid did not affect the catalytic effect of Fe-biochar, which is consistent with the PAA and activated carbon fibers process results (Zhou et al., 2015). The above result indicated that there are active radicals in this process. According to the Eqs. (1)–(3), (22) and (21) of PAA, it can be inferred that there are some radicals like singlet oxygen ($^1\text{O}_2$), $\text{HO}\cdot$, $\text{CH}_3\text{CO}_2\cdot$, $\text{CH}_3\text{CO}_3\cdot$, $\cdot\text{CH}_3$ and $\text{CH}_3\text{CO}_2\cdot$ in Fe-biochar/PAA process. To further clarify the radical species, quenching experiments were performed by using different quenchers. Methanol can react with $\text{HO}\cdot$ and $\text{R-O}\cdot$ effectively (Zhang et al., 2021b). TBA has obvious quenching effect on $\text{HO}\cdot$, but cannot react with $\text{R-O}\cdot$ (Sun et al., 2018; Chen et al., 2019; Yan et al., 2021). 2,4-HD was used as the scavenger for the $\text{R-O}\cdot$ (Kim et al., 2020). As shown in Fig. 5b, addition of TBA only slightly slowed down the removal of acid orange. The result indicated that there are $\text{HO}\cdot$ in this process, but not the main radical species, which was consistent with the results reported in the $\text{Co}_3\text{O}_4/\text{PAA}$, $\text{CoFe}_2\text{O}_4/\text{PAA}$ and UV/PAA processes (Wang et al., 2021a; Zhang et al., 2021a). In contrast, both methanol and 2,4 showed significant inhibitory effects on the removal of acid orange. After adding 1 mM

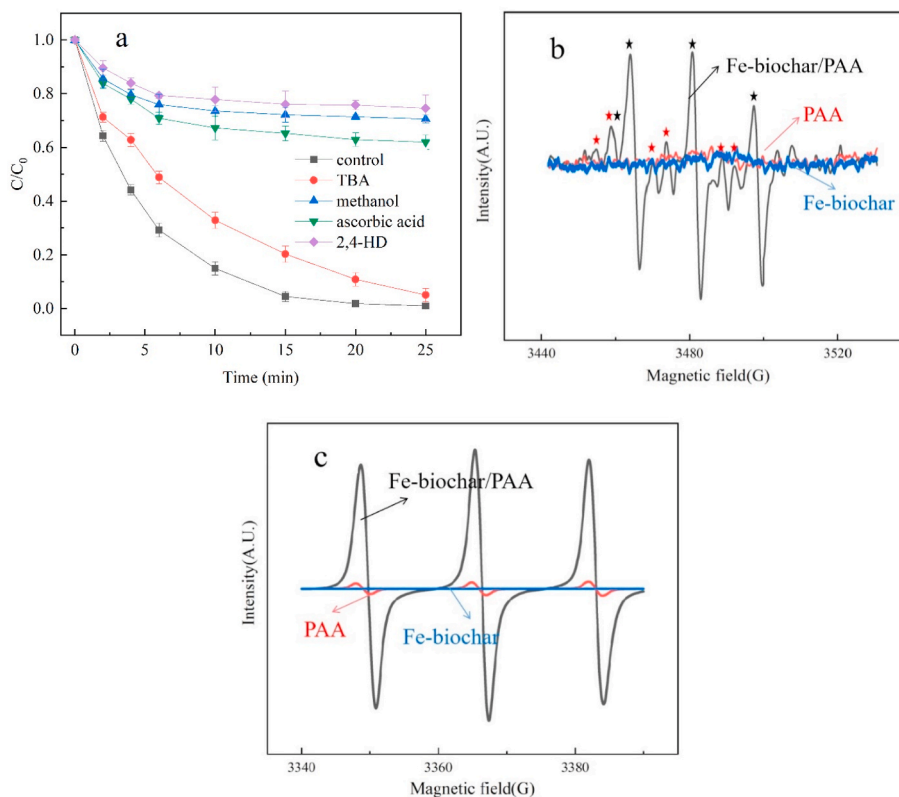


Fig. 5. (a) Effect of different free radical scavengers on the removal of acid orange in the Fe-biochar/PAA process, experimental and simulated EPR spectra of spin-trap adducts in the Fe-biochar/PAA process: (b) DMPO, (c) TEMPO. [acid orange]₀ = 0.143 mM, [PAA]₀ = 1.144 mM, Fe-biochar₀ = 0.3 g/L, pH 7.0. (For interpretation of the references to color in this figure legend, the reader is referred to the Web version of this article.)

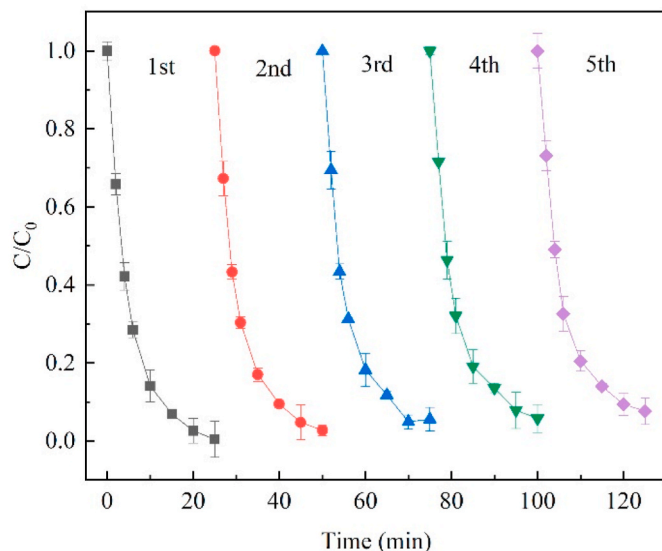


Fig. 6. Reusability of Fe-biochar in the Fe-biochar/PAA process for the removal of acid orange. [acid orange]₀ = 0.143 mM, [PAA]₀ = 1.144 mM, Fe-biochar₀ = 0.3 g/L, pH 7.0. (For interpretation of the references to color in this figure legend, the reader is referred to the Web version of this article.)

methanol and 2,4-HD, the removal rate of acid orange decreased from 99.9% to 29.4% and 25.4%. The decomposition of PAA by 1 mM methanol and 2,4-HD was slightly (Fig. S6), which is not enough to explain the effect of decomposition of PAA. Furthermore, as shown in Fig. S7, excessive PAA did not affect the inhibition of acid orange removal by methanol and 2,4-HD, which indicated that the inhibition

was not attributed to the decomposition of PAA but the radical species of HO· and R-O·. Further result showed that 2,4-HD significantly inhibited the removal of acid orange, indicating that the major radical species were R-O·.

Fig. 5b and c showed EPR spectra of DMPO and TEMPO adducts in the different processes. There were no obvious signals in PAA alone or Fe-biochar alone process whereas strong signals in Fe-biochar/PAA process, which was consistent with PAA/UV-LED/Fe (II) process (Ghanbari et al., 2021). As shown in Fig. 5c, HO· signal (4-line signal, indicated by black stars in Fig. 5c) and carbon-centered radicals signal (6-line signal, indicated by red stars in Fig. 5c) were found which could be attributed to the oxidation of DMPO by CH₃C(O)O· and CH₃C(O)OO·. In addition, ¹O₂ also be found in Fe-biochar/PAA process with a strong intensity signal after addition of TEMPO, suggesting that there is another possible cause for the formation of DMPOX. The DMPO was directly oxidized by ¹O₂ in non-radical pathways. As shown in Fig. 5, the signal intensity of ¹O₂ in Fe-biochar/PAA process was much stronger than that in PAA alone solution, suggesting that ¹O₂ was formed from the catalytic effect on the PAA rather than the self-decomposition of PAA alone. Combining the above radical species scavenging experimental results, it can be concluded that CH₃C(O)O· and CH₃C(O)OO· are the main radical species in Fe-biochar/PAA process, but there may also be non-radical effects in the process of acid orange removal.



3.6. Reusability of Fe-biochar for the removal of acid orange

The reuse rate of the catalyst is an important index to evaluate the performance of the catalyst. As shown in Fig. 6, after the catalyst was recycled for 5 times, the removal rate was still as high as 92.8%, which

was only about 8% less than the first removal rate. The results showed that the use of farmland waste wheat straw combined with iron to prepare iron-loaded biomass carbon can play a significant role in the catalysis of PAA. The XRD patterns of Fe-biochar before and after reaction were shown in Fig. S8, Fe-biochar still appeared characteristic peaks at 44.5°, 38.7°, 35.6°, 51.9° and 56°, indicating that Fe-biochar activation of PAA had little effect on its own crystal form, and also reflected the good stability. Additionally, as shown in Fig. S9, the Fe-biochar/PAA process is selective to degrade pollution, which is attributed to the high selectivity of R-O·. The results also showed that the process had the best removal effect on the bisphenol A of the four pollution, which was owing to the acetyloxy radical showed high reactivity to electron-rich functional groups that contained in these compounds (Kim et al., 2020). In addition, the concentration of the leached iron also was investigated in this research. In this research, the concentration of the leached iron was merely 0.065 mg L⁻¹ after 25min, which is lower than the health reference level of 0.3 mg L⁻¹ in drinking water. Hence, the heterogeneous Fe-biochar/PAA process has great prospects for utilization, and would be economical and without secondary pollution in wastewater/drinking water treatment.

4. Conclusion

In this study, the Fe-biochar catalyst was successfully prepared by a one-step method, and was applied to PAA activation for the first time. The results showed that the Fe-biochar/PAA process degraded acid orange rapidly and had a good effect, which was better than that of metal-free biochar/PAA process. Affected by the metals and the properties of PAA, this process had better removal effect under acidic and neutral conditions. The inhibition on the removal of acid orange was enhanced with the increase of the concentration of humic acids and H₂CO₃⁻ in water, but the effect of Cl⁻ was negligible. The process produced mainly R-O·, HO· and ¹O₂, and quenching experiments suggested that R-O· played a dominant role in the removal process, but there may also be non-radical effects in the process of acid orange removal. Compared with the effective metal catalysis, this process can effectively prevent secondary pollution caused by metal leakage, and the results showed that the iron content in the solution after 25 min of reaction was far lower than the drinking water standard requirements. The Fe-biochar/PAA process was selective for the removal of different pollutants. In addition, the high recycling rate of Fe-biochar also indicated the practicality of the Fe-biochar/PAA process in selectively degrading pollutants. The first proposal of Fe-biochar/PAA process and its remarkable removal effect provide a reference for drinking water or sewage treatment.

Author contribution statement

Changjie Shi: Investigation; Writing; Original Draft; Data Curation. **Yong Wang:** Investigation; Writing; Original Draft. **Kai Zhang:** Review & Editing; Data Curation. **Eric Lichtfouse:** Review & Editing. **Cong Li:** Conceptualization; Supervision; Project administration. **Yunshu Zhang:** Review & Editing.

Declaration of competing interest

The authors declare that they have no known competing financial interests or personal relationships that could have appeared to influence the work reported in this paper.

Data availability

Data will be made available on request.

Acknowledgments

This work is supported by Natural Science Foundation of Shanghai (No.20ZR1438200) and the National Natural Science Foundation of China(No. 51778565).

Appendix A. Supplementary data

Supplementary data to this article can be found online at <https://doi.org/10.1016/j.chemosphere.2022.135686>.

References

- Abd-Elhamid, A.I., Nayl, A.A., 2021. Fabrication and characterization of a novel (GO/PAA/PAM) nanocomposite as effective adsorbent for cationic dyes. *J. Mater. Res. Technol.* 15, 3807–3824.
- Ahmad, M., Usman, A.R.A., Rafique, M.I., Al-Wabel, M.I., 2019. Engineered biochar composites with zeolite, silica, and nano-zerovalent iron for the efficient scavenging of chlortetracycline from aqueous solutions. *Environ. Sci. Pollut. Res.* 26, 15136–15152.
- Ao, X.-w., Eloranta, J., Huang, C.-H., Santoro, D., Sun, W.-j., Lu, Z.-d., Li, C., 2021. Peracetic acid-based advanced oxidation processes for decontamination and disinfection of water: a review. *Water Res.* 188, 116479.
- Cai, M., Sun, P., Zhang, L., Huang, C.-H., 2017. UV/Peracetic acid for degradation of pharmaceuticals and reactive species evaluation. *Environ. Sci. Technol.* 51, 14217–14224.
- Cavallini, G.S., Campos, S.X.d., Souza, J.B.d., Vidal, C.M.d.S., 2013. Comparison of methodologies for determination of residual peracetic acid in wastewater disinfection. *Int. J. Environ. Anal. Chem.* 93, 906–918.
- Chen, S., Cai, M., Liu, Y., Zhang, L., Feng, L., 2019. Effects of water matrices on the degradation of naproxen by reactive radicals in the UV/peracetic acid process. *Water Res.* 150, 153–161.
- Chen, X., Han, Y., Gao, P., Li, H., 2021. New insight into the mechanism of electro-assisted pyrite minerals activation of peroxymonosulfate: synergistic effects, activation sites and electron transfer. *Separ. Purif. Technol.* 274, 118817.
- Coyle, E.E., Ormsbee, L.E., Brion, G.M., 2014. Peracetic acid as an alternative disinfection technology for wet weather flows. *Water Environ. Res.* 86, 687–697.
- das Neves, A.P.N., Carlos, T.D., Bezerra, L.B., Alcenso, W.D., Sarmento, R.A., de Souza, N. L.G.D., Pereira, D.H., Cavallini, G.S., 2021. Carbonate anion photolyzed by solar radiation or combined with peracetic acid to form reactive species for dye degradation. *J. Photochem. Photobiol. A Chem.* 420, 113511.
- Domínguez Henao, L., Turolla, A., Antonelli, M., 2018. Disinfection by-products formation and ecotoxicological effects of effluents treated with peracetic acid: a review. *Chemosphere* 213, 25–40.
- Dong, J., Xu, W., Liu, S., Gong, Y., Yang, T., Du, L., Chen, Q., Tan, X., Liu, Y., 2022. Lignin-derived biochar to support CoFe₂O₄: effective activation of peracetic acid for sulfamethoxazole degradation. *Chem. Eng. J.* 430, 132868.
- Ghanbari, F., Giannakis, S., Lin, K.-Y.A., Wu, J., Madihi-Bidgoli, S., 2021. Acetaminophen degradation by a synergistic peracetic acid/UVC-LED/Fe(II) advanced oxidation process: kinetic assessment, process feasibility and mechanistic considerations. *Chemosphere* 263, 128119.
- Görgüç, A., Gençdağ, E., Okuroğlu, F., Yılmaz, F.M., Bıyık, H.H., Öztürk Köse, S., Erşus, S., 2021. Single and combined decontamination effects of power-ultrasound, peroxyacetic acid and sodium chloride sanitizing treatments on *Escherichia coli*, *Bacillus cereus* and *Penicillium expansum* inoculated dried figs. *LWT* 140, 110844.
- Huang, K., Li, W., Wang, Y., Liu, B., Xu, R., Dai, J., Zheng, X., Yang, N., Qiu, M., Han, L., 2020. Adsorption of acid orange 7 in aqueous solution by biochar from peanut shell supported with clay mineral kaolinite. *Nat. Environ. Pollut. Technol.* 19, 1657–1662.
- Jo, H., Moon, H., Kim, H.J., Hong, J.K., Park, C.J., 2019. Effect of a peroxyacetic acid mixture as green chemical on rice bacterial and fungal pathogens. *J. Plant Pathol.* 101, 661–669.
- Kim, J., Du, P., Liu, W., Luo, C., Zhao, H., Huang, C.-H., 2020. Cobalt/peracetic acid: advanced oxidation of aromatic organic compounds by acetylperoxyl radicals. *Environ. Sci. Technol.* 54, 5268–5278.
- Kim, J., Huang, C.-H., 2021. Reactivity of peracetic acid with organic compounds: a critical review. *ACS ES&T Water* 1, 15–33.
- Kim, J., Zhang, T., Liu, W., Du, P., Dobson, J.T., Huang, C.-H., 2019. Advanced oxidation process with peracetic acid and Fe(II) for contaminant degradation. *Environ. Sci. Technol.* 53, 13312–13322.
- Liu, B., Guo, W., Jia, W., Wang, H., Si, Q., Zhao, Q., Luo, H., Jiang, J., Ren, N., 2021. Novel nonradical oxidation of sulfonamide antibiotics with Co(II)-Doped g-C₃N₄-activated peracetic acid: role of high-valent cobalt-oxo species. *Environ. Sci. Technol.* 55, 12640–12651.
- Mohinuzzaman, M., Yuan, J., Yang, X., Senesi, N., Li, S.-L., Ellam, R.M., Mostofa, K.M.G., Liu, C.-Q., 2020. Insights into solubility of soil humic substances and their fluorescence characterisation in three characteristic soils. *Sci. Total Environ.* 720, 137395.
- Monarca, S., Richardso, S.D., Feretti, D., Grottolo, M., Thruston Jr., A.D., Zani, C., Navazio, G., Ragazzo, P., Zerbini, I., Alberti, A., 2002. Mutagenicity and disinfection by-products in surface drinking water disinfected with peracetic acid. *Environ. Toxicol. Chem.* 21, 309–318.

- Rizzo, L., Agovino, T., Nahim-Granados, S., Castro-Alf rez, M., Fern ndez-Ib n ez, P., Polo-L pez, M.I., 2019. Tertiary treatment of urban wastewater by solar and UV-C driven advanced oxidation with peracetic acid: effect on contaminants of emerging concern and antibiotic resistance. *Water Res.* 149, 272–281.
- Rokhina, E.V., Makarova, K., Golovina, E.A., Van As, H., Virkutyte, J., 2010. Free radical reaction pathway, thermochemistry of peracetic acid homolysis, and its application for phenol degradation: spectroscopic study and quantum chemistry calculations. *Environ. Sci. Technol.* 44, 6815–6821.
- Rothbart, S., Ember, E.E., van Eldik, R., 2012. Mechanistic studies on the oxidative degradation of Orange II by peracetic acid catalyzed by simple manganese(II) salts. Tuning the lifetime of the catalyst. *New J. Chem.* 36, 732–748.
- Silva, W.P.d., Carlos, T.D., Cavallini, G.S., Pereira, D.H., 2020. Peracetic acid: structural elucidation for applications in wastewater treatment. *Water Res.* 168, 115143.
- Sun, P., Zhang, T., Mejia-Tickner, B., Zhang, R., Cai, M., Huang, C.-H., 2018. Rapid disinfection by peracetic acid combined with UV irradiation. *Environ. Sci. Technol. Lett.* 5, 400–404.
- Tang, L., Long, K., Chen, S., Gui, D., He, C., Li, J., Tao, X., 2020. Removal of thiophene sulfur model compound for coal by microwave with peroxyacetic acid. *Fuel* 272, 117748.
- Wang, J., Liao, Z., Iftikhar, J., Shi, L., Chen, Z., Chen, Z., 2017. One-step preparation and application of magnetic sludge-derived biochar on acid orange 7 removal via both adsorption and persulfate based oxidation. *RSC Adv.* 7, 18696–18706.
- Wang, J., Wan, Y., Ding, J., Wang, Z., Ma, J., Xie, P., Wiesner, M.R., 2020a. Thermal activation of peracetic acid in aquatic solution: the mechanism and application to degrade sulfamethoxazole. *Environ. Sci. Technol.* 54, 14635–14645.
- Wang, J., Xiong, B., Miao, L., Wang, S., Xie, P., Wang, Z., Ma, J., 2021a. Applying a novel advanced oxidation process of activated peracetic acid by CoFe₂O₄ to efficiently degrade sulfamethoxazole. *Appl. Catal. B Environ.* 280, 119422.
- Wang, S., Wang, H., Liu, Y., Fu, Y., 2020b. Effective degradation of sulfamethoxazole with Fe²⁺-zeolite/peracetic acid. *Separ. Purif. Technol.* 233, 115973.
- Wang, Z., Shi, H., Wang, S., Liu, Y., Fu, Y., 2021b. Degradation of diclofenac by Fe(II)-activated peracetic acid. *Environ. Technol. (UK)* 42, 4333–4341.
- Wang, Z., Wang, J., Xiong, B., Bai, F., Wiesner, M.R., 2020c. Application of cobalt/peracetic acid to degrade sulfamethoxazole at neutral condition: efficiency and mechanisms. *Environ. Sci. Technol.* 54, 464–475.
- Wu, W., Tian, D., Liu, T., Chen, J., Huang, T., Zhou, X., Zhang, Y., 2020. Degradation of organic compounds by peracetic acid activated with Co₃O₄: a novel advanced oxidation process and organic radical contribution. *Chem. Eng. J.* 394, 124938.
- Yan, T., Ping, Q., Zhang, A., Wang, L., Dou, Y., Li, Y., 2021. Enhanced removal of oxytetracycline by UV-driven advanced oxidation with peracetic acid: insight into the degradation intermediates and N-nitrosodimethylamine formation potential. *Chemosphere* 274, 129726.
- Yang, Z., Yu, A., Shan, C., Gao, G., Pan, B., 2018. Enhanced Fe(III)-mediated Fenton oxidation of atrazine in the presence of functionalized multi-walled carbon nanotubes. *Water Res.* 137, 37–46.
- Yuan, D., Yang, K., Pan, S., Xiang, Y., Tang, S., Huang, L., Sun, M., Zhang, X., Jiao, T., Zhang, Q., Li, B., 2021. Peracetic acid enhanced electrochemical advanced oxidation for organic pollutant elimination. *Separ. Purif. Technol.* 276, 119317.
- Zhang, K., San, Y., Cao, C., Zhang, T., Cen, C., Li, Z., Fu, J., 2021a. Kinetic and mechanistic investigation into odorant haloanisoles degradation process by peracetic acid combined with UV irradiation. *J. Hazard. Mater.* 401, 123356.
- Zhang, K., Zhou, X., Du, P., Zhang, T., Cai, M., Sun, P., Huang, C.-H., 2017. Oxidation of β -lactam antibiotics by peracetic acid: reaction kinetics, product and pathway evaluation. *Water Res.* 123, 153–161.
- Zhang, L., Chen, J., Zhang, Y., Yu, Z., Ji, R., Zhou, X., 2021b. Activation of peracetic acid with cobalt anchored on 2D sandwich-like MXenes (Co@MXenes) for organic contaminant degradation: high efficiency and contribution of acetylperoxyl radicals. *Appl. Catal. B Environ.* 297, 120475.
- Zhao, Z., Li, X., Li, H., Qian, J., Pan, B., 2021. New insights into the activation of peracetic acid by Co(II): role of Co(II)-Peracetic acid complex as the dominant intermediate oxidant. *ACS ES&T Eng.* 1, 1432–1440.
- Zhou, F., Lu, C., Yao, Y., Sun, L., Gong, F., Li, D., Pei, K., Lu, W., Chen, W., 2015. Activated carbon fibers as an effective metal-free catalyst for peracetic acid activation: implications for the removal of organic pollutants. *Chem. Eng. J.* 281, 953–960.

Fe-biochar as a safe and efficient catalyst to activate peracetic acid for the removal of the acid orange dye from water

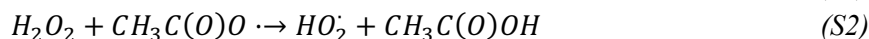
Changjie Shi¹, Yong Wang¹, Kai Zhang¹, Jie Ji¹, Eric Lichtfouse², Cong Li^{1,*}, Yunshu Zhang¹¹ School of Environment and Architecture, University of Shanghai for Science and Technology, Shanghai 200093, China; E-mail: congil@zju.edu.cn² Aix-Marseille Univ, CNRS, IRD, INRAE, CEREGE, Avenue Louis Philibert, Aix en Provence, 13100, France.

Text S1. Sources of the chemical reagents

FeNO₃·9H₂O, H₂O₂ (30% w/w), methanol, NaCl, 70% alcohol, Na₂HCO₃, Humic acid (HA), KI, Na₂S₂O₃, N,N-diethyl-p-phenylenediamine (DPD), H₂SO₄, NaOH, Ascorbic acid (AA), Tertiary Butyl Alcohol (TBA), methanol and 2,4-hexadiene (2,4-HD), sulfamethoxazole (SMX), bisphenol A (BPA) and perfluorooctanoic acid (PFOA) were purchased from Aladdin (Shanghai, China), 5,5-dimethyl-2-pyrrolidone-N-oxyl (DMPO) and 2,2,6,6-Tetramethyl-1-piperidinyloxy (TEMP) were purchased from Enzo Biochem (Inc., New York, USA).

Text S2. Effects of peracetic acid and Fe-biochar concentrations

Effect of PAA dose on the acid orange removal in the Fe-biochar/PAA process was investigated in Fig.S2. Compared with the process of Fe-biochar alone (removal rate=44.5%), the removal rate of acid orange was increased to 82.7%- 99.9% in the Fe-biochar/PAA process with the concentration of PAA changed, indicating that PAA play an important role in the process of Fe-biochar/PAA process removal. As shown in Fig.S2a, when the dose of PAA increased from 0.143 to 1.144mM, the removal rate also increased. Higher concentrations of PAA will provide more reactive species for degrading acid orange. But when the concentration of PAA was higher than 1.144mM, the result was opposite. The reaction rate constant had the same changes (Table.S2). In this research, PAA concentration of 1.144mM had the largest reaction rate constant ($k_{obs}=0.2574 \text{ min}^{-1}$). When the concentration of PAA is too high, the excess PAA will inhibit the production of reactive species (Dong et al., 2022). In addition, as the PAA concentration increases, the concentration of coexisting H₂O₂ also increases in the reaction solution(Wu et al., 2020). Fig.S3 showed the effect on removal of acid orange when the H₂O₂ concentration in the process was increased. The result suggested that excess H₂O₂ will inhibit the generation of R-O· (mainly CH₃C(O)OO· and CH₃C(O)O·) (Eq. S1 and S2) and then affect the removal of acid orange. Active radicals are mainly generated by PAA, while excess H₂O₂ inhibits the decomposition of PAA in the reaction solution (Chen et al., 2019).



The effect of Fe-biochar concentration on the removal of acid orange in Fe-biochar/PAA process was investigated. In Fig.S2b, the concentration of acid orange hardly changed in the absence of Fe-biochar process and the removal of AOXI by PAA alone can be negligible. However, the concentration of acid orange decreased significantly after adding Fe-biochar to the reaction process. The experimental result showed that the removal rates of acid orange increased with increment of Fe-biochar dosages, indicating PAA required Fe-biochar as a catalyst to promote the generation of active radicals (Rokhina et al., 2013). In addition, more Fe-biochar will accelerate the removal of acid orange from Table.S3. The inconspicuous removal of acid orange when the dosage of Fe-biochar was higher than 0.3g/L was likely owing to the dosages of 0.3g/L were enough to accelerate PAA generate radicals. The results indicated that when the initial concentration of Fe-biochar is 0.3g/L under this experimental condition, acid orange has been degraded completely in 25 min, that is, the removal rate reaches 99.8%.

Table S1 Properties of biochar and Fe-biochar

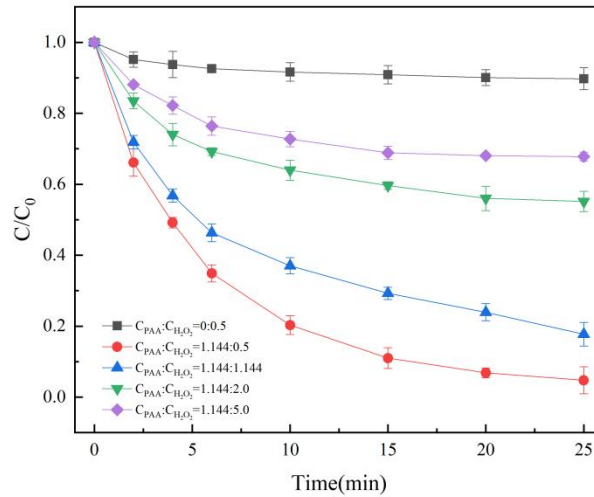
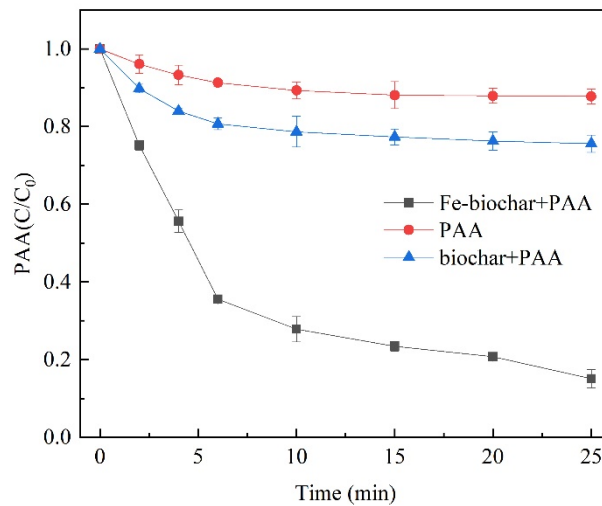
Test content	biochar	Fe-biochar
BET surface area	146.15m ² /g	128.36 m ² /g
Pore volume	0.02 cm ³ /g	0.29 cm ³ /g
Pore size	2.5 nm	8.0 nm

Table S2 k_{obs} of different PAA doses

PAA doses (mM)	0.143	0.286	0.715	1.144	1.432	7.151
k_{obs} (min^{-1})	0.0798	0.0944	0.1212	0.2574	0.1404	0.0697

Table S3 k_{obs} of different Fe-biochar doses

Fe-biochar doses (g/L)	0	0.1	0.2	0.3	0.4	0.5
k_{obs} (min^{-1})	0.0051	0.031	0.1135	0.2486	0.3015	0.3516

**Figure S1.** Acid orange removal in the Fe-biochar/PAA process with different concentrations of H_2O_2 . $[\text{acid orange}]_0 = 0.143 \text{ mM}$, $\text{Fe-biochar}_0 = 0.3 \text{ g/L}$, $\text{pH } 7.0$ **Figure S2.** Decomposition of PAA in the Fe-biochar/PAA, biochar/PAA and PAA alone processes. $[\text{acid orange}]_0 = 0.143 \text{ mM}$, $\text{PAA}_0 = 1.144 \text{ mM}$, $\text{Fe-biochar}_0 = 0.3 \text{ g/L}$, $\text{pH } 7.0$

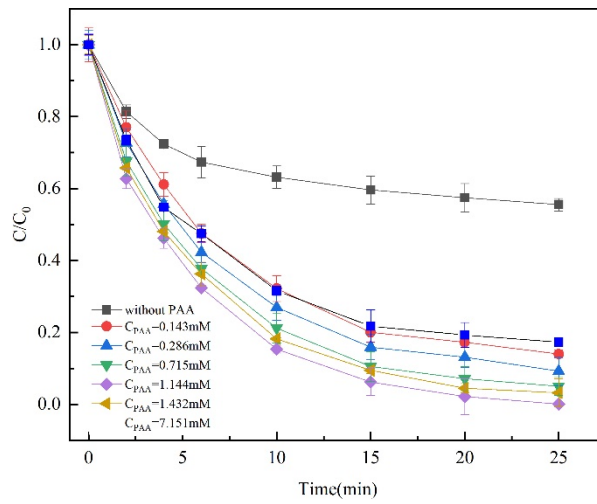


Figure S3. Effect of initial PAA dose, on the removal of acid orange in the Fe-biochar/PAA process. $[\text{acid orange}]_0 = 0.143 \text{ mM}$, $\text{Fe-biochar}_0 = 0.3\text{g/L}$, $\text{pH } 7.0$

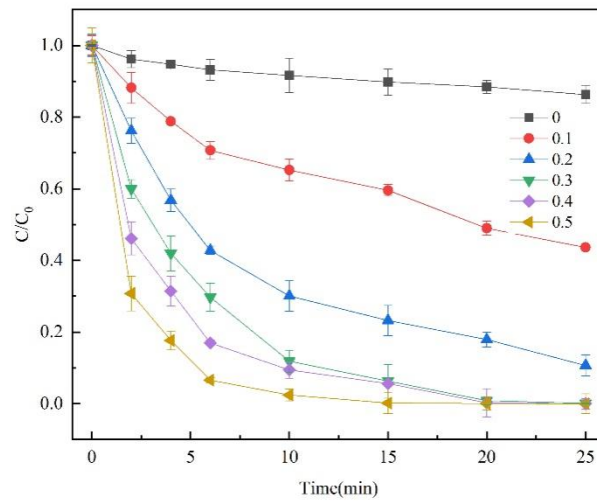


Figure S4. Effect of Fe-biochar dose on the removal of acid orange in the Fe-biochar/PAA process. $[\text{acid orange}]_0 = 0.143 \text{ mM}$, $\text{PAA}_0=1.144\text{mM}$, $\text{pH } 7.0$

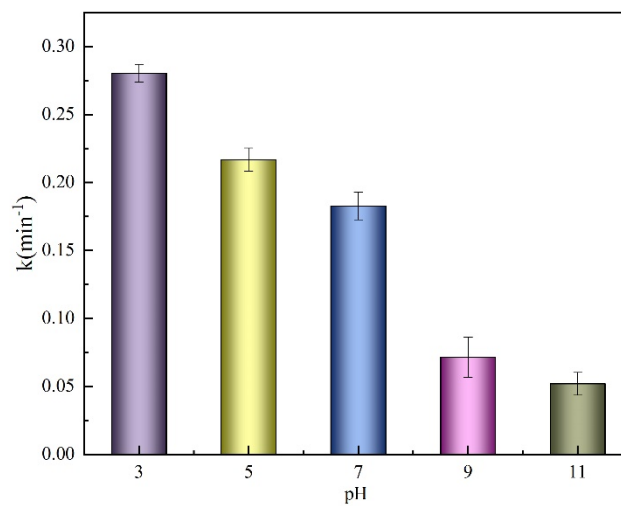


Figure S5. The corresponding kinetic constants of different pH in the Fe-biochar/PAA process

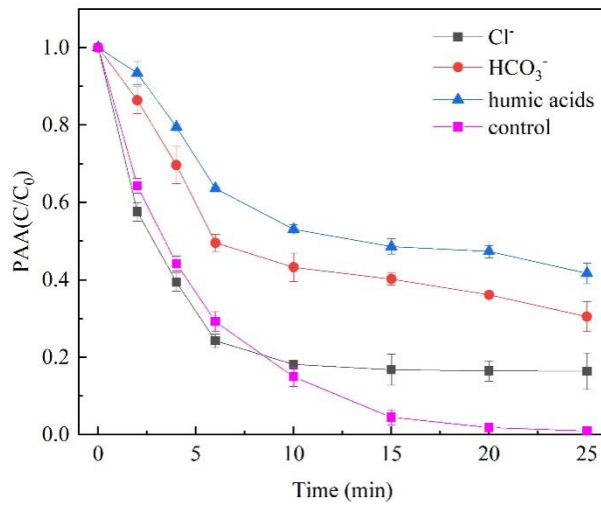


Figure S6. Decomposition of PAA in the Fe-biochar/PAA process with and without humic acids, HCO_3^- and Cl^- .
 $[\text{acid orange}]_0 = 0.143 \text{ mM}$, $[\text{PAA}]_0 = 1.144 \text{ mM}$, $\text{Fe-biochar}_0 = 0.3 \text{ g/L}$, $\text{pH } 7.0$

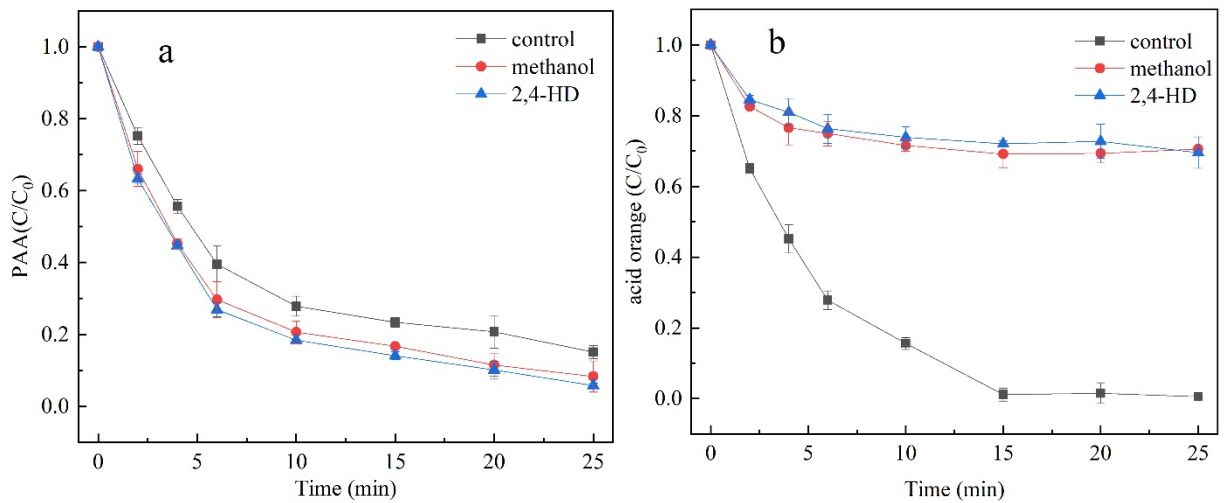


Figure S7. (a) Peracetic acid (PAA) consumption and (b) acid orange removal in the Fe-biochar/PAA process with and without the presence of methanol, 2,4-HD. $[\text{acid orange}]_0 = 0.143 \text{ mM}$, $[\text{PAA}]_0 = 1.144 \text{ mM}$, $\text{Fe-biochar}_0 = 0.3 \text{ g/L}$, $\text{pH } 7.0$

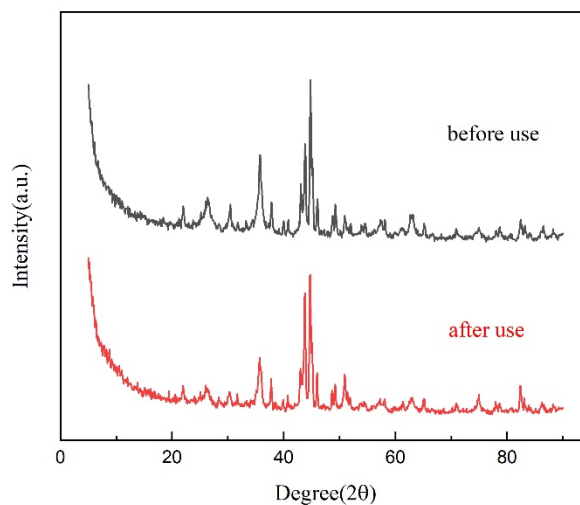


Figure S8. The XRD patterns of Fe-biochar before and after reaction

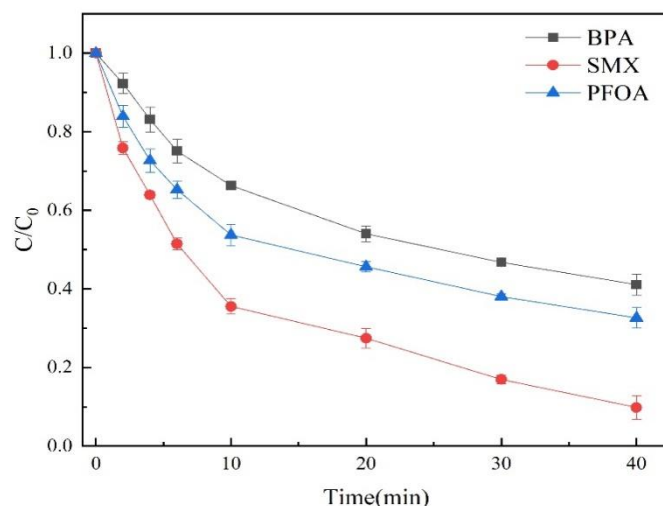


Figure S9. Removal of BPA, SMX and PFOA by the Fe-biochar/PAA process. $[\text{acid orange}]_0 = 0.143 \text{ mM}$, $[\text{PAA}]_0 = 1.144 \text{ mM}$, $\text{Fe-biochar}_0 = 0.3 \text{ g/L}$, $\text{pH } 7.0$

Chen, S., Cai, M., Liu, Y., Zhang, L., Feng, L., 2019. Effects of water matrices on the degradation of naproxen by reactive radicals in the UV/peracetic acid process. *Water Research* 150, 153-161.

<https://doi.org/10.1016/j.watres.2018.11.044>

Dong, J., Xu, W., Liu, S., Gong, Y., Yang, T., Du, L., Chen, Q., Tan, X., Liu, Y., 2022. Lignin-derived biochar to support CoFe_2O_4 : Effective activation of peracetic acid for sulfamethoxazole degradation. *Chemical Engineering Journal* 430, 132868.

<https://doi.org/10.1016/j.cej.2021.132868>

Rokhina, E.V., Makarova, K., Lahtinen, M., Golovina, E.A., Van As, H., Virkutyte, J., 2013. Ultrasound-assisted MnO_2 catalyzed homolysis of peracetic acid for phenol degradation: The assessment of process chemistry and kinetics. *Chemical Engineering Journal* 221, 476-486.

<https://doi.org/10.1016/j.cej.2013.02.018>

Wu, W., Tian, D., Liu, T., Chen, J., Huang, T., Zhou, X., Zhang, Y., 2020. Degradation of organic compounds by peracetic acid activated with Co_3O_4 : A novel advanced oxidation process and organic radical contribution. *Chemical Engineering Journal* 394, 124938.

<https://doi.org/10.1016/j.cej.2020.124938>